# Effects of cloud microphysics on the universal performance of neural network radiation scheme

Hwan-Jin Song* and Park Sa Kim

National Institute of Meteorological Sciences, Korea Meteorological Administration, Jeju-do, Republic of Korea

Submitted to Geophysical Research Letters (16 February 2022)

**Key Points**

- Effects of 15 microphysics schemes on radiation emulator were examined for the period of one year over the Korean peninsula.
- Radiation emulator obtained from real case trainings was applied to the 2-dimentional ideal case simulation to test the universal application of the emulator.
- Maintaining stability and accuracy of radiation emulator on microphysics changes was confirmed in both real and ideal cases.

---

** Corresponding author's address*
Hwan-Jin Song
National Institute of Meteorological Sciences,
63568, Seogwipo-si, Jeju-do, Republic of Korea
E-mail: hwanjinsong@gmail.com

**Abstract**

The stability on cloud microphysics changes is essential for the use of radiation emulator in an operational weather forecasting model with frequent updates. This study examined the effect of 15 microphysics schemes on radiation emulator for real and ideal cases. In the real case, although the forecast errors against control run were increased with different microphysics schemes to the trained scheme, the forecast error of 2-m temperature was rather improved by 0.9–5.4% compared with observations. The radiation emulator for the real case was applied to the 2-dimentional idealized squalline simulation to test the universal application of the emulator, resulting that forecast errors of heating rates and fluxes for 14 microphysics schemes were increased by 8.6–41.3% than the trained scheme. The errors can be further reduced by 26.5–50.4% with the use of compound parameterization. Therefore, the stability and accuracy of radiation emulator on microphysics changes was confirmed.

**Keywords:** WRF, RRTMG, radiation, microphysics, neural network, emulator

**Plain Language Summary**

The machine learning emulator for radiation process has been developed to reduce the computational cost in numerical weather prediction model. It is useful to faster alarm for severe weather events (e.g., heavy snowfall, flood, and typhoon). By the way, frequent updates of operational model have been an obstacle to apply the radiation emulator because the machine learning approach is based on a statistical relationship in the past version of model. Among many components of weather forecasting model, cloud microphysics can significantly affect the stability of radiation emulator. In severe case, the entire numerical model can blow up while producing unphysical forecast outputs. This study investigated the effects of 15 microphysics schemes on radiation emulator for both real and ideal cases. The real case simulation was performed for one-year period over the Korean peninsula, and the emulator developed in the real case was implemented to the ideal case simulation to further test the universal applicability of radiation emulator. In both real and ideal cases, this study maintained the stability and accuracy of radiation emulator on microphysics changes. This result can therefore contribute to provide an important guidance for the operational use of radiation emulator in a weather forecasting model.

## 1. Introduction

Cloud is the most important among atmospheric components in determining radiation processes. Regarding the radiative effect of clouds, longwave (LW) cooling and shortwave (SW) warming are evidently found above and below the cloud top, respectively (Zhang et al., 2017; Roh and Song, 2020). Along with cloud fraction, cloud size and optical properties can be further considered to compute atmospheric heating rates and fluxes (Bae et al., 2016; Thompson et al., 2016; Fovell et al., 2016; Bae and Park, 2019). For example, effective radius and water path profiles for snow, cloud ice, and cloud liquid are input parameters within the Rapid Radiative Transfer Model for GCMs (RRTMG; Iacono et al., 2008), which is one of the most popular radiation parameterizations.

Despite the importance of cloud microphysics on radiation process, the most radiation emulators in numerical forecast models have been developed in ignoring the effect of cloud microphysics (Krasnopolsky et al., 2005, 2008, 2010; Belochitski et al., 2011; Roh and Song, 2020; Belochitski and Krasnopolsky, 2021; Song and Roh, 2021; Song et al., 2021, 2022), while the emulators were quite useful in significant speedup (tens of times) compared with the RRTMG or RRTMG-K (Baek, 2017) schemes. These are two main reasons for such trend reflecting cloud microphysics. If microphysics variables (e.g., effective radius and water path profiles) are further considered, the number of input variables becomes approximately twice; then it reduces the speedup of emulator by half. By the way, despite of the slowdown, accuracy improvement may not be sufficient because the uncertainty of microphysics variables can influence the stability of radiation emulator. Belochitski and Krasnopolsky (2021) (hereafter, BK21) examined the robustness of radiation emulator by applying training results based on the Climate Forecast System (CFS) model into the Global Forecast System (GFS) model. They found stable results for the use of radiation emulator although there were many changed from the CFS to the GFS for dynamical core, physics grids, planetary

boundary layer scheme, radiation scheme's version, the treatment of trace gases, and mean $CO_2$ concentration. However, they experienced that use of radiation emulator produced unphysical values of outgoing LW radiation (OLR) for the GFS simulation using the GFDL scheme (Zhou et al., 2019) because the emulator was trained under the influence of the Zhao–Carr microphysics (Zhao and Carr, 1997) in the CFS model. These suggest the change of microphysics scheme induced the greatest uncertainty among sensitivity experiments in BK21. This issue needs to be solved in order to facilitate the use of radiation emulator in operational numerical weather prediction (NWP) model with frequent updates of cloud scheme.

We suspect two reasons for the failure in BK21 on microphysics changes. As noted in BK21, the Zhao–Carr microphysics considered one prognostic variable (total condensate of cloud water and ice), whereas the GFDL microphysics predicted six variables (cloud water, cloud ice, rain, snow, graupel, and cloud fraction). Thus, the interaction between radiation and clouds based on simple microphysics (Zhao–Carr) can be much different with that with complex microphysics (GFDL). In addition, the small number of training sets (200,000 input-output pairs) used in Krasnopolsky et al. (2010) and BK21 may not be able to express the complexity processes between radiation and clouds that exist in nature. In order to solve these problems, this study utilizes the neural network (NN) radiation scheme developed in Song et al. (2022) (hereafter, S22) with 60-fold speed for radiation process compared with the RRTMG-K. The number of training sets used in S22 was 720-fold larger than 200,000 pairs. This emulator was also developed under the indirect influence of the complex WDM7 microphysics that predicts 6-class mixing ratios and 3-class number concentration (Bae et al., 2019). This study investigates whether or not that the emulator maintains universal stability on additional 14 microphysics schemes for a year period over the Korean peninsula. The application of emulator based on real-case training into 2D idealized squalline simulation is

also examined. These efforts will provide an important guidance for the operational use of radiation emulator in the NWP model.

## 2. Data and Methods

This study inherited radiation emulator and validation framework used in the previous study (Song et al., 2022). Those were publicly released in https://doi.org/10.5281/zenodo.5638436. They considered two simulation frameworks (real vs. ideal cases) using 5-km resolution (234×282 vs. 201 grids), 39 vertical layers (40 levels up to 50 hPa), and 20-s time step. The real case simulation was based on the Korea Local Analysis and Prediction System (KLAPS) model (Shin et al., 2022) for short-range operational forecasting in the Korea Meteorological Administration (KMA). In this study, the part of data assimilation was replaced by the European Center for Medium-Range Weather Forecasts Reanalysis v5 (ERA5) reanalysis (Hersbach et al., 2020). The remaining model part of the KLAPS is equivalent to the Advanced Research Weather Research and Forecasting (WRF-ARW) model (Skamarock et al., 2019). The real case was integrated by 168 hours for 48 weekly cases initialized from $1^{st}$, $8^{th}$, $15^{th}$, $22^{th}$ day of each month for the year 2020. The ideal case is the 2D idealized squalline experiment embedded within the WRF model. This experiment is a popular framework in developing microphysics parameterization (Hong and Lim, 2006; Morrison et al., 2009; Lim and Hong, 2010; Morrison and Milbrandt, 2015; Bae et al., 2019). We used the default initial sounding with low-level heat forcing in the WRF model.

The radiation emulator of S22 consisted of 96 categories (LW/SW, 12 months, land/ocean, and clear/cloud) from individual training for the 96-type sets. Training sets were obtained for the period of 2009–2019 and prognostic evaluation with the emulator was performed for the year 2020. Weight and bias coefficients from the NN training with the Stochastic Weight Averaging (SWA; Izmailov et al., 2018) were implemented in the WRF model by replacing

140 the RRTMG-K code (*module_ra_rrtmg_swk.F*). Here, single hidden layer and 90 neurons
141 were considered (see S22 for detail explanations). This radiation emulator was 60-fold faster
142 than the RRTMG-K. In the emulator, microphysics variables were excluded from inputs
143 while bulk cloud fraction was only used. However, the outputs in the training set (heating
144 rates and fluxes) were already affected by cloud effective radius and water path from
145 microphysics. Thus, the effect of radiation on microphysics was implicitly considered in the
146 emulator. Because S22 used the WDM7 microphysics scheme (Bae et al., 2019) in generation
147 of training sets, we cannot guarantee the stability of radiation emulator when it was applied to
148 other microphysics schemes. This study focuses on the stability of radiation emulator for 14
149 additional microphysics schemes (Lin, Eta, WSM6, Goddard, Thompson, Milbrandt,
150 Morrison, CAM5.1, SBU-YLin, WDM6, NSSL, NSSL-1m, Thompson_A, and P3). The
151 number of *mp_physics* (used in the WRF modeling), abbreviations of schemes, brief
152 descriptions, and references were given in Table S1 (supporting information). The
153 precipitation at convection-permitting scale (i.e., 5 km) is mostly determined by cloud
154 microphysics, there is a huge difference between microphysics schemes (Song and Sohn,
155 2018; Tapiador et al., 2019). Note that the relationship between RRTMG-K and WDM7 was
156 projected to the radiation emulator results using 14 additional microphysics schemes (i.e., no
157 re-learning for 14 microphysics schemes). The simulation results from real cases were
158 evaluated with the control run using the RRTMG-K and WDM7, as well as surface
159 temperature and precipitation (gauge-radar merged product) observations in South Korea.
160 As a more challenging attempt, the radiation emulator developed in the real case was
161 implemented to the ideal case simulation along with the use of 15 microphysics schemes. As
162 noted in S22, the uncertainty of radiation emulator for the ideal case was more rapidly
163 amplified compared with the real case because the ideal case had relatively weak constraint
164 by various dynamics and physics based on theoretical equations. In S22, the ideal case

showed more large RMSEs for LW/SW fluxes (10.58 W $m^{-2}$ and 96.56 W $m^{-2}$) than the real case for 48 weekly cases (8.90 W $m^{-2}$ and 60.22 W $m^{-2}$) despite of short forecast time (24 hours) compared with the real case (168 hours), indicating the ideal case is a good framework to test the behavior of radiation emulator in an extreme case. The 96-type emulators of S22 can be further separated to 24 categories (land-ocean and 12 months) because LW-SW and clear-cloud are essential for one simulation. Among 24 categories, we chose land and July for the ideal simulation by considering the land condition over the United States and the maximum incident solar radiation. Because the emulator in S22 was over the Korean peninsula, it had a strong dependency with seasons, especially for solar zenith angle. In this study, we slightly modified vertical grid intervals (40 levels up to 50 hPa) to follow the real case. The ideal simulations with the radiation emulator were evaluated with multiple control runs using the RRTMG-K and 15 microphysics schemes.

## 3. Results and Discussion

Figure 1 represents weekly time series (48 cases) of RMSEs for LW/SW fluxes, 2-m air temperature, and the accuracy of precipitation forecast with the threshold of 0.5 mm. Here, the fluxes indicate the average of upward fluxes at the top/bottom as well as downward flux at the bottom. The RMSEs for LW/SW fluxes were derived by comparing between the control run using the RRTMG-K and WDM7 schemes and radiation emulator results, whereas 2-m temperature and precipitation results were evaluated with surface observations in South Korea. The RMSEs for fluxes were calculated from 226×274 horizontal grids and 168 forecast hours with a 3-h interval (3,467,744 points for each case) for the year 2020. The LW/SW fluxes showed a strong seasonal variability along with the largest RMSEs for summer season (Figs. 1a–b). It is due to humid and cloudy environments over the Korean peninsula as a part of the summer monsoon (Song and Sohn, 2015). The deviations of RMSEs with microphysics schemes were also the largest in the wet season. The RMSE for

LW flux was larger in winter than spring and autumn (Fig. 1a), whereas this pattern was not found in SW flux (Fig. 1b). Strong variability of skin temperature in dry season can be related with the feature for LW flux, but it is not input variable for SW flux. In a different way, the RMSEs for 168 forecast hours were given as the time series in Fig. S1 (supporting information). The RMSEs of LW/SW fluxes were substantially amplified with the increased forecast time. Both LW/SW fluxes indicated a strong dependency with diurnal cycle, while SW flux was more sensitivity with solar activity because solar zenith angle is the most important input for SW radiation. Total statistics for 48 cases (derived from 166,451,712 points) were given in Fig. 2. We should remember that the radiation emulator in S22 was trained under the influence of cloud-radiation interaction between WDM7 and RRTMG-K. Thus, the RMSE deviations with microphysics schemes in Figs. 1a–b and 2a–b indicated the degree of similarity to the WDM7. In fact, the WDM7 scheme was developed from the WDM6 (Lim and Hong, 2010) by adding hail category, and the WDM6 was the double-moment version of the WSM6 (Hong and Lim, 2006). These two schemes were the most and the second most close to the WDM7 with the lowest error, resulting the second and third lowest RMSEs for LW/SW fluxes. The largest errors for LW/SW fluxes were found in the use of NSSL scheme, indicating that this scheme was much different with the WDM7. Overall, the RMSEs of LW/SW fluxes were distributed over the ranges of 8.90–16.45 W $m^{-2}$ and 60.22–100.64 W $m^{-2}$, respectively. Compared with the WDM7, the mean RMSEs with the use of 14 microphysics schemes were increased by 59.29% and 38.79%, respectively. We can expect these deviations would be more reduced if those were compared with control run for each microphysics scheme. Although the RMSEs may be increased with the use of different microphysics, we had not experienced for producing unphysical OLRs such as in BK21, indicating the radiation emulator in this study was more mature for a universal application.

The evaluation results to surface observations in Figs. 1c–d are quite interesting. The deviation with microphysics experiments for RMSEs of 2-m temperature was not much high, except for June and August. Interestingly, the emulator result with the use of WDM7 tended to show the largest error in June, August, and May (Fig. 1c). In the time series for forecast hours, the WDM7 experiment also indicated the largest error after 60 hour among schemes (Fig. S1c in the supporting information). As a result, the WDM7 experiment exhibited the largest RMSE of 2.26 K for 2-m temperature (Fig. 2). It was 0.13 K larger than the NSSL experiment showing the minimum error. Coincidentally, the NSSL experiment also showed the largest deviation for LW/SW fluxes with the WDM7 experiment. The forecast accuracy of precipitation tended to be reduced in July–August (Fig. 1d) and with the increased forecast hour (Fig. S1d in the supporting information), while the deviation with microphysics schemes was quite small. In contrast to 2-m temperature, the WDM7 experiment showed the second highest performance for precipitation forecast (0.9046); it was slightly higher than the mean accuracy (0.8969) of 14 microphysics schemes (Fig. 2). Because radiation process greatly affects surface temperature whereas it has an indirect effect on determining precipitation, the substantial improvement of temperature forecast by 0.9–5.4% should be more emphasized than the slight degradation of precipitation forecast (maximum 1.7%),. More important is that the universal stability of radiation emulator was verified even if different microphysics schemes were used. This is an essential condition for the use of radiation emulator in the operational NWP model. Note that dynamics and other physics parameterizations except for cloud microphysics did not directly affect the radiation process.

Although BK21 failed to show the universal applicability of radiation emulator on microphysics changes, their attempt for different models (CFS training → GFS testing) deserves its novelty. For similar concept, this study further examined whether that the stability of radiation emulator is maintained when the trained result in the real case was

applied to the 2D idealized squalline simulation. Note that the ideal case is more uncertain than the average of real case simulations. Evolutionary features of RMSEs for LW/SW heating rates and fluxes were given in Fig. 3 and Fig. S2 in the supporting information. Each experiment was evaluated with each control run based on different microphysics scheme. The RMSEs for LW heating rate and flux tended to be increased with forecast time, while SW heating rate and flux showed the largest error around the noon. Similar to the real case simulation, the evolutional pattern of the WDM7 experiment was close with the WSM6 and WDM6 experiments. By the way, the RMSEs of LW heating rate and flux from the experiment using the Goddard scheme (Tao et al., 1989) were rapidly increased after hour 16 (Fig. 3a and Fig. S2a). These features were also connected with the increased error of SW flux after noon (Fig. S2b). Reader may doubt “blow up” of the NWP model for the Goddard experiment, such as unphysical OLR value in BK21. However, the Goddard experiment produced OLRs within the physical range although it was much different with the control run after hour 16 (Figs. S3a–b in the supporting information). The WRF model tends to stop during the integration when simulation results are too unstable and unrealistic; we have not experienced this shutdown for both real and ideal cases. Looking the mean cloud fraction and precipitation patterns of control runs, the Goddard experiment showed a unique evolutionary pattern with rapid increases of cloud and precipitation after hour 14 (Figs. S3c–d in the supporting information). The mean cloud fraction for the Goddard experiment was 3.6-fold larger than the average of other experiments after hour 16. The abundant clouds for the Goddard experiment can explain the rapid increase of RMSEs for LW heating rate and flux shown in Fig. 3 and Fig. S2. In addition, the Eta experiment showing the second highest cloud fraction and precipitation exhibited the second highest error of LW heating rate (Fig. 3a). Sudden increases of LW heating rate and flux before hour 4 (Fig. 3c and Fig. S2c) in the experiment using the CAM5.1 scheme (Neale et al., 2012) were also thought to be related

265 with early cloud formation for the scheme (Fig. S3c). These are characteristics of control runs;
266 thus, it is difficult to regard only as the stability issue of radiation emulator.

267 Although the stability of radiation emulator was secured, the improvement of forecast
268 error is the ultimate goal of the emulator study. In order to further improve accuracy, we can
269 utilized the concept of compound parameterization (CP) designed by Krasnopolsky et al.
270 (2008) that allows return to the original parameterization when the predicted error of SW
271 heating rate exceeds 0.5 K $day^{-1}$. The inclusion of CP to the NN emulator makes slowdown
272 compared with the emulator only (i.e., 60-fold speedup), while forecast accuracy can be
273 significantly improved. Song et al. (2021) examined the effect of CP on radiation emulator
274 developed in Song and Roh (2021). Because training datasets and NN training method were
275 changed from Song and Roh (2021) to S22, we modified the CP algorithm to the radiation
276 emulator of S22 while maintaining the same structure with Song et al. (2021). The CP was
277 only applied to cloud area where more than 1.0341 K $day^{-1}$ of LW heating rate and 0.4820 K
278 $day^{-1}$ of SW heating rate were expected in night and day, respectively. The thresholds were
279 emphatically determined by considering the 3-fold slowdown to the radiation emulator for
280 training sets. The computation time for the ideal case simulation may be changed due to
281 different cloud characteristics and uncertainties of emulator with cloud microphysics. Table
282 S2 in the supporting information exhibited that the use of CP produced 2.77-fold slowdown
283 for radiation process compared with the NN emulator using the WDM7 scheme; thus total
284 reduction of computation time was decreased from 84.7% to 57.7%. The mean slowdowns
285 with the use of CP were distributed over 2.75 to 5.71-fold with different microphysics
286 schemes. Because the radiation scheme is infrequently utilized than the time step of model in
287 the operational NWP model, the reduction of total computation time would not be much
288 different between NN and NN+CP emulators. If radiation scheme is called every $15^{th}$ time
289 step and it is occupied 20% of total computation, the difference in total computation between

NN and NN+CP (with 4-fold slowdown) is only 1%. Instead of this slowdown, the accuracy of emulator results can be much enhanced as shown in Figs. 3c–d and Figs. S2c–d. In particular, the amplification of LW errors after hour 16 for the Goddard experiment was weakened (Fig. 3d and Fig. S2d), while the uncertainty of emulator in relation with abundant cloud condition was not fully solved, implying the necessary of more active CP to further reduces error. Total statistics for 201 grids and 4,320 time steps (24 hours with 20-s interval) between NN and NN+CP were represented in Fig. 4 and Fig. S4 in the supporting information. The RMSEs of LW/SW heating rates and LW/SW fluxes were reduced by 38.99%, 50.39%, 26.54%, and 28.66%, respectively, with the addition of CP. The improvements of RMSEs with the use of CP were the largest in the Milbrandt experiment (41–60%). The mean RMSEs of 14 microphysics experiments for NN experiments were 8–41% larger RMSEs compared with WDM7 experiment, whereas NN+CP experiments showed 2–13% smaller RMSEs to the WDM7. It suggested that the uncertainty of radiation emulator with the use of different microphysics schemes was greatly reduced with the use of CP. Therefore, the CP as well as the NN emulator can be usefully utilized as an option for the operational use of radiation emulator in the NWP model.

## 4. Summary and Conclusions

This study examined the effects of cloud microphysics on the stability and accuracy of radiation emulator in the NWP model. Two-type simulations (real and ideal cases) were considered to evaluate the universal performance of radiation emulator using additional 14 microphysics schemes beside the WDM7 scheme used in the NN training. The real case simulation over Korea and the ideal case were integrated by 168 hours (for 48 weekly cases of the year 2020 and 24 hours, respectively. Because microphysics variables were excluded from inputs of the emulator, it can become an uncertainty factor influencing the stability of the emulator. In comparison with the control run with the WDM7 in the real case, the mean

RMSEs of LW/SW fluxes with the use of 14 microphysics schemes were increased by 59.29% and 38.79% compared with the WDM7 experiment. Although the RMSEs were increased by the use of different microphysics, evaluation results with surface observations showed that the forecast accuracy of 2-m temperature was improved by 0.9–5.4% whereas that of precipitation was slightly degraded by the maximum 1.7%, compared with the WDM7 experiment. The radiation emulator based on real-case training was further applied to the 2D idealized squalline simulation. In comparison with the control runs with different microphysics schemes, emulator result exhibited the mean RMSEs of LW/SW heating rates and fluxes for 14 microphysics schemes were increased by 8.6–41.3%, compared with the WDM7 experiment. These RMSEs can be further reduced using the use of the CP by 26.5–50.4%, indicating the CP is an option to further secure the stability of emulator. Among microphysics experiments, the Goddard showed the unique pattern with a rapid increase of forecast error after hour 16; but it was mostly affected by abundant clouds of the control run.

This study is particularly valuable in terms of overcoming the BK21's failure on microphysics changes in the universal application of radiation emulator. It was thought to be by virtue of the maturity of the emulator with the use of more training sets and complex microphysics scheme. Although the forecast error with different microphysics schemes can be increased, it did not emerge as an instability issue (i.e., blow up of model). The evaluation with surface observations also showed stable results while maintaining the forecast accuracy of 2-m temperature and precipitation. It is an essential condition for the use of radiation emulator in the operational NWP model with frequent updates. Although this study showed the possibility of universal radiation emulator in both real and ideal cases, its application to global regions is restricted because maximum solar zenith angle over Korea used in the SW training is less than that over tropics. Future expansion into global model along with more training datasets is required to improve the universality of radiation emulator.

## Acknowledgements

This work was funded by the KMA Research and Development Program “Development of AI techniques for weather forecasting” under Grant (KMA2021-00121).

## Data Availability Statement

The datasets and sources codes were obtained from https://doi.org/10.5281/zenodo.5638436. The modified codes for ideal case simulation are available in https://doi.org/10.5281/zenodo.6033618.

## References

Bae, S. Y., Hong, S.-Y., & Lim, K.-S.S. (2016). Coupling WRF Double-Moment 6-class microphysics schemes to RRTMG radiation scheme in Weather Research Forecasting model. *Advances in Meteorology,* 2016, 1–11. https://doi.org/10.1155/2016/5070154.

Bae, S. Y., & Park, R.-S. (2019). Consistency between the cloud and radiation processes in a numerical forecasting model. *Meteorology and Atmospheric Physics,* 131, 1429–1436, https://doi.org/10.1007/s00703-018-0647-9.

Bae, S. Y., Hong, S.-Y., & Tao, W.-K. (2019). Development of a single-moment cloud microphysics scheme with prognostic hail for the Weather Research and Forecasting (WRF) model. *Asia-Pacific Journal of Atmospheric Sciences,* 55, 233–245. https://doi.org/10.1007/s13143-018-0066-3.

Baek, S. (2017). A revised radiation package of G-packed McICA and two-stream approximation: Performance evaluation in a global weather forecasting model. *Journal of Advances in Modeling Earth Systems,* 9, 1628–1640. https://doi.org/10.1002/2017MS000994.

Belochitski, A., Binev, P., DeVore, R., Fox-Rabinovitz, M., Krasnopolsky, V., & Lamby, P. (2011). Tree approximation of the long wave radiation parameterization in the NCAR CAM global climate model. *Journal of Computational and Applied Mathematics*, 236, 447–460. https://doi.org/10.1016/j.cam.2011.07.013.

Belochitski, A., & Krasnopolsky, V. (2021). Robustness of neural network emulations of radiative transfer parameterizations in a state-of-the-art General Circulation Model. *Geoscientific Model Development,* 14, 7425–7437. https://doi.org/10.5194/gmd-2021-114.

Fovell, R. G., Bu, Y. P., Corbosiero, K. L., Tung, W., Cao, Y., Kuo, H.-C., Hsu, L., & Su, H. (2016) Influence of cloud microphysics and radiation on tropical cyclone structure and motion. *Meteorological Monographs,* 56, 11.1-11.27. https://doi.org/10.1175/amsmonographs-d-15-0006.1

Hersbach, H., Bell, B., Berrisford, P., Hirahara, S., Horányi, A., Muñoz-Sabater, J., Nicolas, J., Peubey, C., Radu, R., Schepers, D., Simmons, A., Soci, C., Abdalla, S., Abellan, X., Balsamo, G., Bechtold, P., Biavati, G., Bidlot, J., Bonavita, M., Chiara, G., Dahlgren, P., Dee, D., Diamantakis, M., Dragani, R., Flemming, J., Forbes, R., Fuentes, M., Geer, A., Haimberger, L., Healy, S., Hogan, R. J., Hólm, E., Janisková, M., Keeley, S., Laloyaux, P., Lopez, P., Lupu, C., Radnoti, G., Rosnay, P., Rozum, I., Vamborg, F., Villaume, S., Thépaut, J.-N. (2020). The ERA5 global reanalysis. *Quarterly Journal of the Royal Meteorological Society*, 146, 1999– 2049. https://doi.org/10.1002/qj.3803.

Hong, S.-Y., & Lim, J.-O. (2006). The WRF single-moment 6-class microphysics scheme (WSM6). *Journal of the Korean Meteorological Society*, 42, 129–151.

Iacono, M. J., Delamere, J. S., Mlawer, E. J., Shephard, M. W., Clough, S. A., & Collins, W. D. (2008). Radiative forcing by long-lived greenhouse gases: Calculations with the AER radiative transfer models. *Journal of Geophysical Research*, 113, D13103. https://doi.org/10.1029/2008JD009944.

Izmailov, P. Podoprikhin, D., Garipov, T., Vetrov, D., and Wilson, A. G. (2018). Averaging weights leads to wider optima and better generalization. *Conference on Uncertainty in Artificial Intelligence (UAI) 2018.* https://arxiv.org/abs/1803.05407.

Krasnopolsky, V. M., Fox-Rabinovitz, M. S., & Chalikov, D. V. (2005). New approach to calculation of atmospheric model physics: Accurate and fast neural network emulation of longwave radiation in a climate model. *Monthly Weather Review*, 133, 1370–1383. https://doi.org/10.1175/MWR2923.1.

Krasnopolsky, V. M., Fox-Rabinovitz, M. S., Tolman, H. L., & Belochitski, A. A. (2008). Neural network approach for robust and fast calculation of physical processes in numerical environmental models: Compound parameterization with a quality control of larger errors. *Neural Networks*, 21, 535–543. https://doi.org/10.1016/j.neunet.2007.12.019.

Krasnopolsky, V. M., Fox-Rabinovitz, M. S., Hou, Y. T., Lord, S. J., & Belochitski, A. A. (2010). Accurate and fast neural network emulations of model radiation for the NCEP coupled Climate Forecast System: Climate simulations and seasonal predictions. *Monthly Weather Review*, 138, 1822–1842. https://doi.org/10.1175/2009MWR3149.1.

Lim, K. S., & Hong, S.-Y. (2010). Development of an effective double-moment cloud microphysics scheme with prognostic cloud condensation nuclei (CCN) for weather and climate models. *Monthly Weather Review*, 138, 1587–1612. https://doi.org/10.1175/2009mwr2968.1.

Morrison, H., Thompson, G., & Tatarskii, V. (2009). Impact of cloud microphysics on the development of trailing stratiform precipitation in a simulated squall line: Comparison of one- and two-moment schemes. *Monthly Weather Review*, 137, 991–1007. https://doi.org/10.1175/2008mwr2556.1.

Morrison, H., & Milbrandt, J. A. (2015). Parameterization of cloud microphysics based on the prediction of bulk ice particle properties. Part I: Scheme description and idealized tests. *Journal of the Atmospheric Sciences*, 72, 287–311. https://doi.org/10.1175/JAS-D-14-0065.1.

Neale, R. B., et al. (2012), Description of the NCAR Community Atmosphere Model (CAM5.0), NCAR/TN-486+STR, NCAR, Boulder, Colorado, USA. [Available at http://www.cesm.ucar.edu/models/cesm1.0/cam/docs/description/cam5_desc.pdf.].

Roh, S., & Song, H.-J. (2020). Evaluation of neural network emulations for radiation parameterization in cloud resolving model. *Geophysical Research Letters,* 47, e2020GL089444. https://doi.org/10.1029/2020GL089444.

Shin, H.-C., Ha, J.-H., Ahn, K. D., Lee. E. H., Kim, C. H., Lee. Y. H., & Clayton, A. (2022). An overview of KMA's operational NWP data assimilation system. In: Park, S. K. & Xu. L. (eds) Data Assimilation for Atmospheric, Oceanic and Hydrologic Applications (Vol. IV). Springer, Cham. https://doi.org/10.1007/978-3-030-77722-7_26.

Skamarock, W. C., Klemp, J. B., Dudhia, J., Gill, D. O., Liu, Z., Berner, J., Wang, W., Powers, J. G., Duda, M. G., Barker, D. M., & Huang, X.-Y. (2019). A description of the Advanced Research WRF model version 4. *NCAR Technical Notes.* https://doi.org/10.5065/1DFH-6P97.

Song, H.-J., & Sohn, B. J. (2015). Two heavy rainfall types over the Korean peninsula in the humid East Asian summer environment: A satellite observation study. *Monthly Weather Review*, 143, 363–382. https://doi.org/10.1175/MWR-D-14-00184.1.

Song, H.-J., & Sohn, B. J. (2018). An evaluation of WRF microphysics schemes for simulating the warm-type heavy rain over the Korean peninsula. *Asia-Pacific Journal of Atmospheric Sciences*, 54, 1–12. https://doi.org/10.1007/s13143-018-0006-2.

Song, H.-J., & Roh, S. (2021). Improved weather forecasting using neural network emulation for radiation parameterization. *Journal of Advances in Modeling Earth Systems,* 13, e2021MS002609. https://doi.org/10.1029/2021MS002609.

Song, H.-J., Roh, S., & Park, H. (2021). Compound parameterization to improve the accuracy of radiation emulator in a numerical weather prediction model. *Geophysical Research Letters*, 48, e2021GL095043. https://doi.org/10.1029/2021GL095043.

Song, H.-J., Roh, S., Lee, J., Nam, G., Yun, E., Yoon, J., & Kim, P. S., (2022). Benefits of stochastic weight averaging in developing neural network radiation scheme for numerical weather prediction. *Journal of Advances in Modeling Earth Systems,* https://doi.org/10.1002/essoar.10508964.1 (in revision).

Tao, W.-K., Simpson, J., & McCumber, M. (1989). An ice-water saturation adjustment. *Monthly Weather Review,* 117, 231–235. https://doi.org/10.1175/1520-0493(1989)117<0231:AIWSA>2.0.CO;2.

Tapiador, F. J., Sánchez, J.-L., & García-Ortega, E. (2019). Empirical values and assumptions in the microphysics of numerical models. *Atmospheric Research,* 215, 214–238. https://doi.org/10.1016/j.atmosres.2018.09.010.

Thompson, G., Tewari, M., Ikeda, K., Tessendorf, S., Weeks, C., Otkin, J., & Kong, F. (2016) Explicitly-coupled cloud physics and radiation parameterizations and subsequent evaluation in WRF high-resolution convective forecasts. *Atmospheric Research,* 168, 92–104. https://doi.org/10.1016/j.atmosres.2015.09.005.

Zhang, K., Randel, W. J., & Fu, R. (2017). Relationships between outgoing longwave radiation and diabatic heating in reanalyses. *Climate Dynamics*, 49, 2911–2929. https://doi.org/10.1007/s00382-016-3501-0.

Zhao, Q., & Carr, F. H. (1997). A prognostic cloud scheme for operational NWP models. *Monthly Weather Review*, 125, 1931–1953. https://doi.org/10.1175/1520-0493(1997)125<1931:APCSFO>2.0.CO;2.

Zhou, L., Lin, S., Chen, J., Harris, L. M., Chen, X., & Rees, S. L. (2019). Toward convective-scale prediction within the next generation global prediction system. *Bulletin of the American Meteorological Society*, 100, 1225–1243. https://doi.org/10.1175/BAMS-D-17-0246.1.

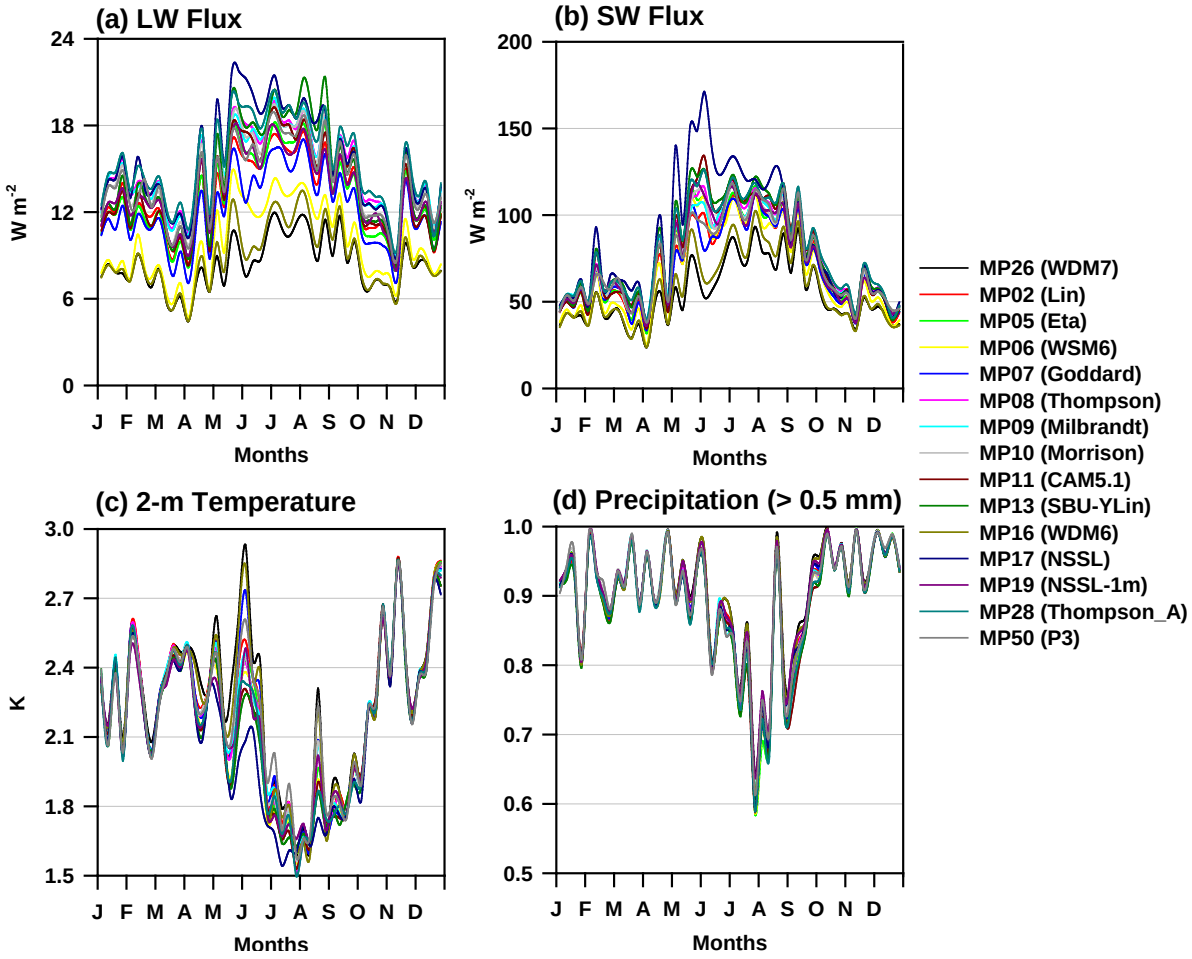


**Figure 1.** Weekly times series of RMSEs for (a) LW flux and (b) SW flux compared with the control run (RRTMG-K & WDM7), as well as (c) 2-m air temperature and (d) the accuracy of precipitation forecast (the threshold of precipitation is 0.5 mm) compared with surface observations over the Korean peninsula. Mean statistics over the whole domain and 1-week forecast with a 3-h interval were represented for 48 cases of the year 2020. Each color indicates the used microphysics schemes.

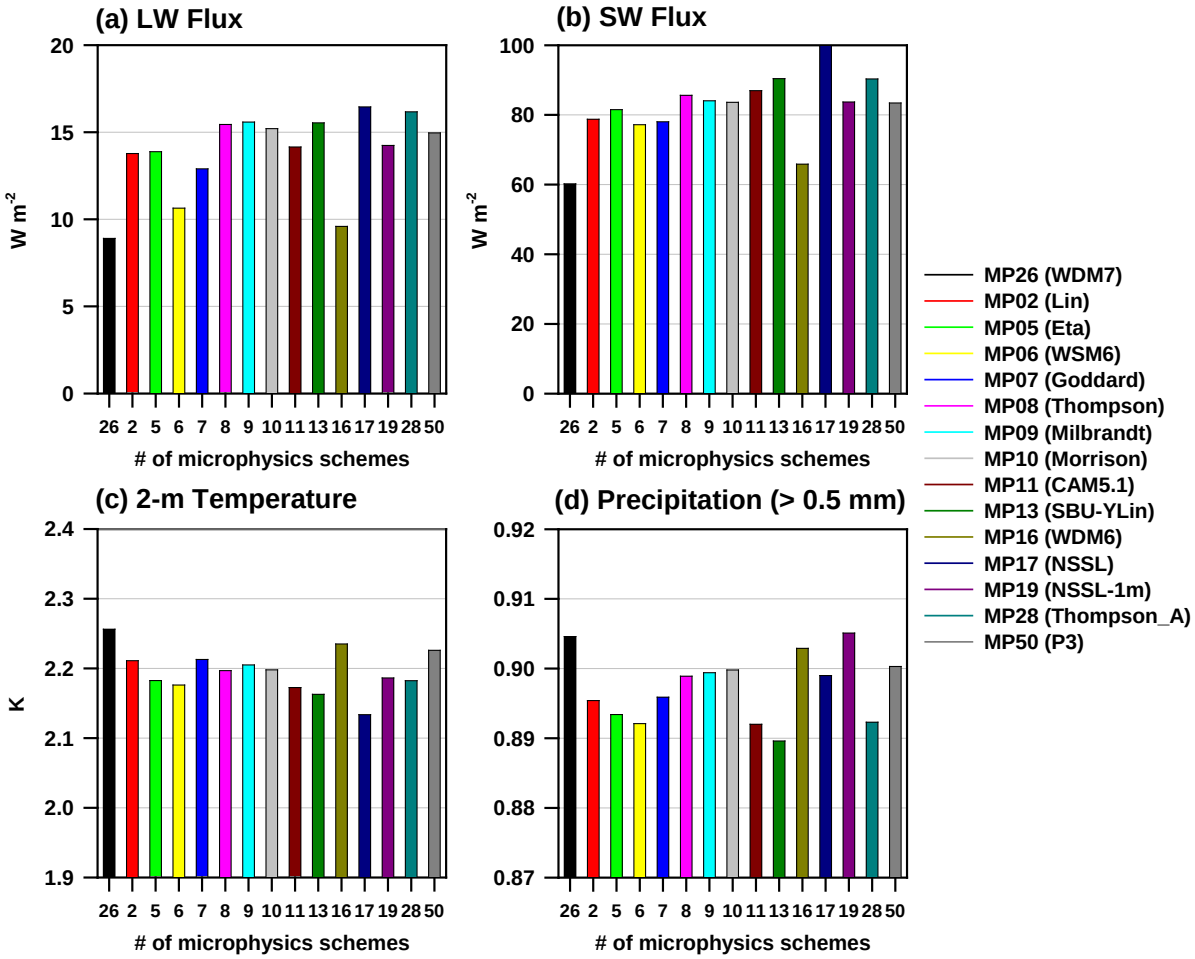


**Figure 2.** Same as Fig. 1, but for the average of total 48 cases.

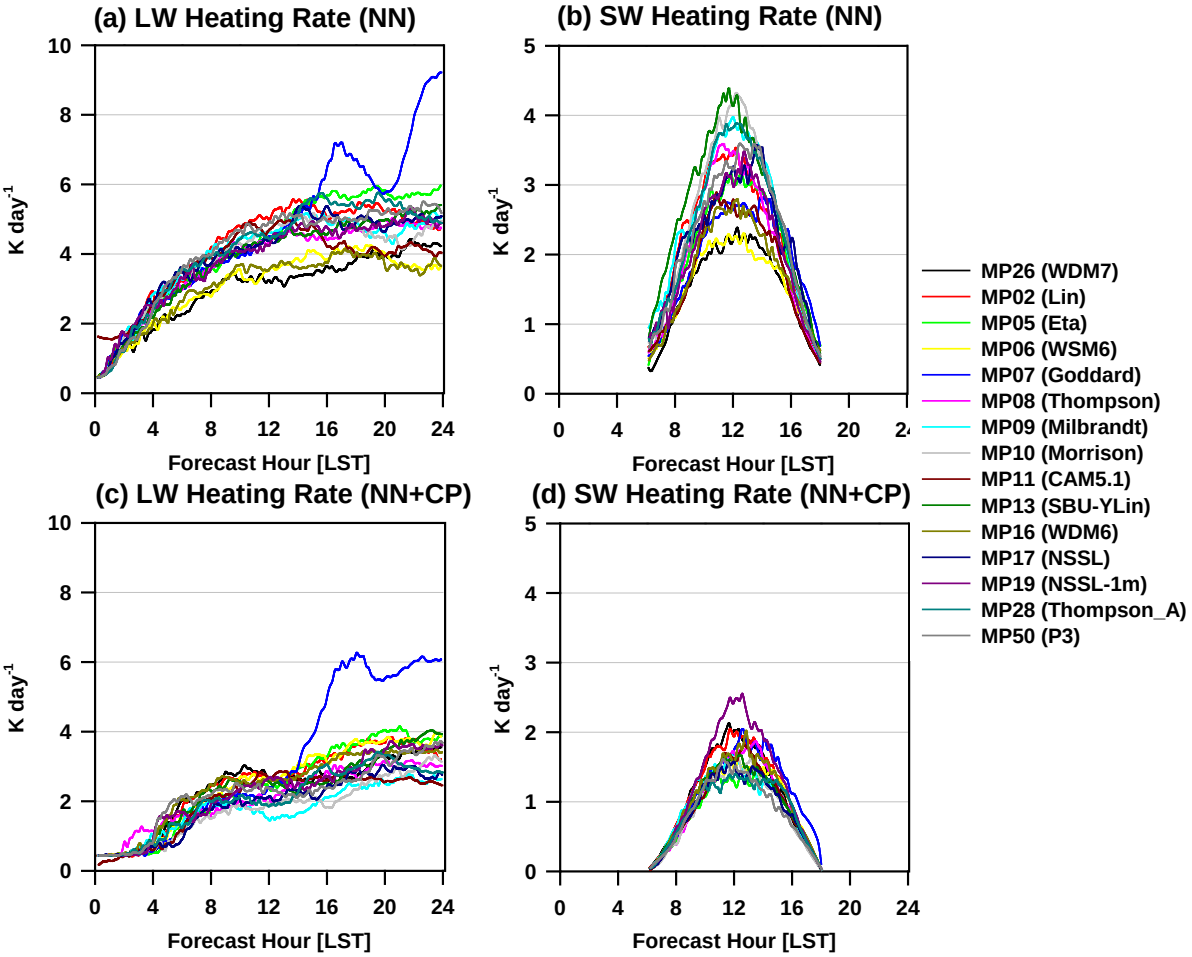


**Figure 3.** Times series of RMSEs for (a) LW heating rate and (b) SW heating rate with the use of the radiation emulator (NN), as well as (c) LW heating rate and (d) SW heating rate with the additional use of the compound parameterization (NN+CP) over the two-dimensional idealized squalline simulation. The horizontal mean statistics at each 10-min interval were represented. Each color indicates the used microphysics schemes.

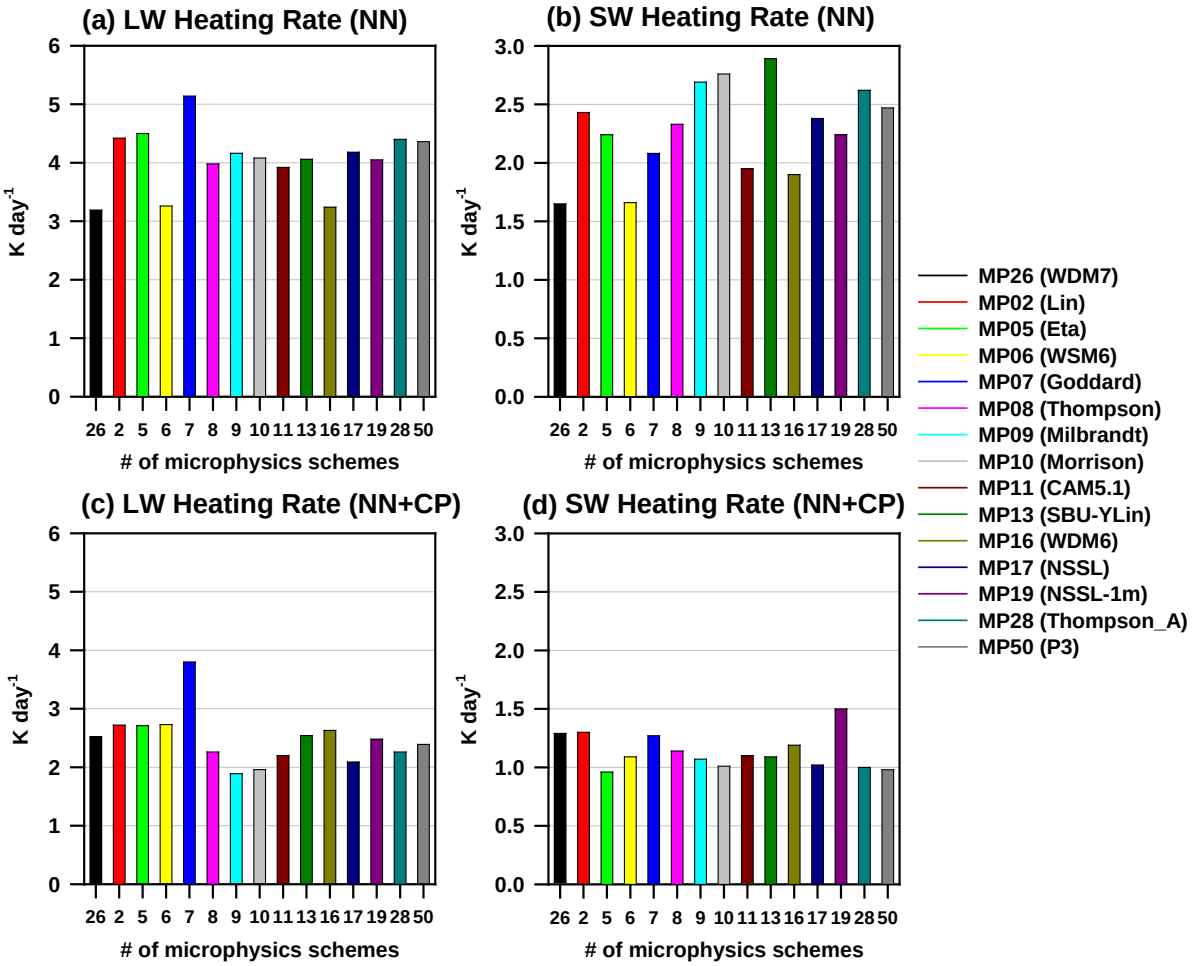


**Figure 4.** Same as Fig. 3, but for total statistics for both horizontal and temporal variations.